

Fast T-wave detection with annotation of P and T waves in the MIT-BIH arrhythmia database

Mohamed Elgendi¹

1 Department of Computing Science, University of Alberta, Edmonton, Canada

E-mail: moe.elgendi@gmail.com

Abstract

There are limited studies on the automatic detection of T waves in arrhythmic electrocardiogram (ECG) signals. This is perhaps because there is no available arrhythmia dataset with annotated T waves. Here, the annotation of the well-known MIT-BIH arrhythmia database is discussed and provided. Moreover, a simple fast method for detecting T waves is introduced. There is a need for developing numerically-efficient algorithms to accommodate the new trend toward battery-driven ECG devices and to analyze long-term recorded signals in a time-efficient manner. A typical T-wave detection method has been reduced to a basic approach consisting of two moving averages and dynamic thresholds calibrated by clinical knowledge. In contrast to complex methods, it can be easily implemented in a digital filter design.

Introduction

According to the World Health Organization, cardiovascular diseases (CVDs) are the number one cause of death globally; more people die annually from CVDs than from any other cause. An estimated 17.3 million people died from CVDs in 2008, representing 30% of all global deaths. Of these deaths, an estimated 7.3 million were due to coronary heart disease and 6.2 million were due to stroke. Thus, medical researchers have placed significant importance on cardiac health research. This has led to a strong focus on technological advances with respect to cardiac function assessment. One such research pathway is the improvement of conventional cardiovascular diagnosis technologies used in hospitals and clinics.

The most common clinical cardiac test is electrocardiogram (ECG) analysis as it is simple, risk-free, and inexpensive [1]. The signal of each heart beat contains five main events: P wave, Q wave, R wave, S

wave, and T-wave (as shown in Figure 1). Each event (wave) has its corresponding peak. The analysis of ECG signals for monitoring or diagnosis requires the detection of these events. Once an event has been detected, the corresponding signal can be extracted and analyzed in terms of its amplitude (peak), morphology, energy and entropy distribution, frequency content, intervals between events, and other more complex parameters. The detection of R peaks and QRS complexes has been extensively investigated over the past two decades. Conversely, T-event detection has not been investigated as much as QRS detection, and the T-event detection problem is still far from being solved [2]. Reliable T-wave detection is more difficult than QRS complex detection for several reasons, including low amplitudes, low signal-to-noise ratio (SNR), amplitude and morphology variability, and possible overlapping of the P wave and T wave.

Advances in technology have led to much change in the way we collect, store, and diagnose ECG signals, especially the use of mobile phones to implement the clinical routine of ECG analysis into everyday life [3-7]. Thus, in the near future, it is expected that Holter devices, which are traditionally used for ECG analysis in the clinic, will be replaced by portable battery-operated devices, such as mobile phones, in the near future [8,9]. The reason for this is that Holter devices do not detect arrhythmias automatically in real time.

In order to develop fast robust algorithms for detecting arrhythmia in ECG collected by portable, wearable, and battery-driven devices, we need fully annotated arrhythmia ECG signals first as a benchmark for evaluation. Unfortunately, the MIT-BIH Arrhythmia Database [10] includes *only* the annotations of R peaks. Therefore, in this study, an initiative has been taken to annotate T waves in the MIT-BIH Arrhythmia Database [10,11]. Moreover, a new fast robust algorithm consisting of two moving averages that are calibrated by a clinical knowledge base is presented.

Materials and Methods

Data Used

Several standard ECG databases are available for the evaluation of QRS detection algorithms for ECG signals. Most of these databases contain annotated files for R peaks but not for T-waves. In this study, the P and T peaks of the MIT-BIH Arrhythmia Database [10,11] will be annotated, then used for evaluation for the following reasons:

1. The MIT-BIH Database contains 30-minute recordings for each patient, which is considerably longer than the records in many other databases, such as the Common Standards for Electrocardiography database, which contains 10-second recordings [12].
2. The MIT-BIH Arrhythmia Database contains records of normal ECG signals and records of ECG signals that are affected by non-stationary effects, low SNR, premature atrial complexes, premature ventricular complexes, left bundle blocks, and right bundle blocks. This provides an opportunity to test the robustness of T-wave detection methods.
3. The database contains 23 records (the 100 series) that were chosen at random from a set of more than 4,000 24-hour Holter tapes, and 25 records (the 200 series) that were selected from the same set, including a variety of rare and clinically important ECG segments [10]. Several records in the 200 series have abnormal rhythms and QRS morphologies and they suffer from a low SNR. These issues are expected to present significant difficulties for any ECG signal analysis algorithm [10].

Annotation is a difficult task due to inter-annotator discrepancy, as two annotators will never agree completely on what and how to annotate the T waves in each record. However, Figures 2, 3, and 4 demonstrate a preliminary annotation of T waves for different beats in the MIT-BIH Arrhythmia Database. The annotation file of P and T waves can be downloaded from <http://www.elgendi.net/databases.htm>.

T-waves Detection Algorithm

In this study, a fast robust knowledge-based T-waves detection algorithm will be discussed and evaluated. The algorithm is based on the framework proposed by Elgendi for detecting QRS complexes in ECG signals [13, 14], for detecting systolic waves in photoplethysmogram signals [15], and detecting a waves in the acceleration photoplethysmogram (PPG) signals [16–19]. The same approach will be used here to detect T waves. The method consists of three main stages: pre-processing (bandpass filtering and squaring), feature extraction (generating potential blocks using two moving averages), and classification (thresholding). The structure of the algorithm is given in Figure 5.

Bandpass Filter

Based on Sahambi *et al.* [20] and our investigation shown in Figure 6, most of the energy of T waves lies below 10 Hz. Thus, a zero-phase second-order Butterworth filter, with bandpass 0.5–10 Hz, is

implemented to remove the baseline wander and high frequencies that do not contribute to the T waves. The output of the zero-phase Butterworth filter applied to the PPG signal will produce a filtered signal $x[n]$.

QRS Removal

To make the T waves the dominant feature of the signal, the QRS complex is removed. Therefore, R peaks must be detected before applying the T-waves algorithm. Fortunately, R peaks are annotated in the MIT-BIH Arrhythmia Database. Removing the QRS complex duration is performed by setting the signal to zero for the duration of the QRS complex. As the duration of the QRS complex varies with the heart beat type, a clinical database is required to remove the QRS according to its type. Roskamm and Csapo divided the ECG into four categories: compensation, reset, interpolation, and reentry [21], as shown in Figure 7. Based on their analysis, a rule-based knowledge representation of different types of QRS complexes is established for QRS removal; however, an extra category is added to capture complex arrhythmias (repetitive, bigeminy, or trigeminy), as demonstrated in Figure 8. The output of this stage will produce signal $y[n]$.

During the QRS removal, the RR interval that satisfied each category is saved and referred to as RR_i , where i is the category type (compensation, reset, interpolation, reentry, and complex arrhythmias). The normalized RR intervals average in each category is calculated as $M_i = (\sum_{j=1}^l RR_{i,j})/f_s$, where l is the number of RR intervals saved in category i , and f_s is the sampling frequency (a frequency of one beat per second).

Generating Blocks of Interest

Blocks of interest are generated using two event-related moving averages that demarcate the areas of T waves, which was first introduced in Ref [22]. The particular method used to generate blocks of interest has been mathematically shown to detect a waves [17], QRS complexes [13], and systolic waves in PPG signals [15]. In this procedure, the first moving average (MA_{peak}) is used to emphasize the peak of the T-wave area, as the dotted signal shown in Figure 9, and is given by

$$MA_{\text{peak}}[n] = \frac{1}{W_1}(y[n - (W_1 - 1)/2] + \cdots + y[n] + \cdots + y[n + (W_1 - 1)/2]), \quad (1)$$

where W_1 represents the window size of approximately the shortest T-wave (peak) duration in ECG signals. The initial value for W_1 of 70 ms is determined by Trahanias [23]. However, as the ECG signals may contain different arrhythmias the value of W_1 will be calculated relative to the most frequent RR intervals in all five categories ($k = \max_i M_i$). Then, the value of $W_1 = (70 \text{ ms}) * k$, and the result is rounded to the nearest odd integer. The second moving average ($MA_{T\text{wave}}$) is used to emphasise the T-wave area to be used as a threshold for the first moving average, shown as a dashed signal Figure 9, and is given by

$$MA_{T\text{wave}}[n] = \frac{1}{W_2} (y[n - (W_2 - 1)/2] + \dots + y[n] + \dots + y[n + (W_2 - 1)/2]), \quad (2)$$

where W_2 represents the window size of approximately the smallest T-wave duration. The initial value for W_2 of 140 ms is determined by Laguna *et al.* [24]. However, as the ECG signals may contain different arrhythmias, the value of W_2 will be calculated relative to the most frequent RR intervals in all five categories (k). Then, the value of $W_2 = (140 \text{ ms}) * k$, and the result is rounded to the nearest odd integer.

Thresholding

In this stage, the blocks of interest are generated by comparing the MA_{peak} signal with $MA_{T\text{wave}}$. Many blocks of interest will be generated, some of which will contain the T wave and others will contain P waves, U waves, and noise. Therefore, the next step is to reject blocks that result from noise. Rejection is based on the relative positions of P and T waves to R peaks and anticipated peak width.

To determine whether the detected blocks contain T waves or not, the number of blocks in each consecutive RR interval is counted. A threshold based on the distance of the maximum point within a block to the R peak is applied to distinguish P waves from T waves and noise, as shown in Figure 10. The search regions for T waves in terms of time occurrence with respect to the current R peak (R_i) and the next R peak (R_{i+1}) are calculated as

$$R_i T_{min} = D_{min} * R_i R_{i+1}, \quad (3)$$

$$R_i T_{max} = D_{max} * R_i R_{i+1}, \quad (4)$$

where $R_i T_{min}$ represents the minimum dynamic interval between the T wave and the current R peak,

$R_i T_{max}$ represents the maximum dynamic interval between the T wave and the current R peak, while $R_i R_{i+1}$ represents the interval between R_i and R_{i+1} . The exact values for D_{min} and D_{max} are 170 ms and 800 ms, respectively, as determined by Schimpf *et al.* [25] to represent the minimum RT durations for subjects with arrhythmia and maximum RT duration for healthy subjects.

After applying the relative-position thresholds, there are three possibilities for the number of detected blocks within the area of interest:

1. **Zero:** if there is no block detected, it means the algorithm failed to detect a T wave in the current RR interval.
2. **One:** if there is one detected block, it means the algorithm succeeds in detecting T wave, P and T waves are most likely merged within one block, which is marked as a circle with a black asterisk inside (see Figures 11 (i, j)).
3. **More than one:** if there are multiple detected blocks, it means one of the detected blocks contains T waves. However, in this work the nearest block to the current R peak is considered a T wave.

All detected blocks go through a durational threshold to reject the undesired blocks called THR_1 , which rejects the blocks that contain P wave, U wave, and noise. By applying the THR_1 threshold, the accepted blocks will contain T peaks only,

$$THR_1 = W_1. \quad (5)$$

As discussed, the threshold THR_1 corresponds to the anticipated T-wave duration. If a block is wider than or equal to THR_1 , it is classified as a T wave. If not, it will be classified as noise. The last stage is to find the maximum absolute value within each block to detect the peak of T wave. Consecutive R peaks are shown in Figure 9 to demonstrate the idea of using two moving averages to generate blocks of interest. Not all of the blocks contain potential T waves; some blocks are caused by noise and need to be eliminated. Blocks that are smaller than the expected width for the T-wave duration are rejected. The rejected blocks are considered to be noisy blocks, and the accepted blocks are considered to contain a T wave. The detected T-wave peaks are compared to the annotated T-wave peaks to determine whether they were detected correctly. The search range for the true T-wave peak is fixed to ± 50 ms for both databases, to ensure consistency of comparison.

Results

The algorithm was evaluated using the MIT-BIH database. The T waves were detected successfully even when the P and T waves are merged in arrhythmia ECG signals that are affected by: high-frequency noise, baseline wander, normal sinus rhythm (NSR), left bundle branch block (LBBB), right bundle branch block (RBBB), premature ventricular contraction (PVC), and premature atrial contraction (PAC). All of the reasons for detection failure are described below. High-frequency noise results from the instrumentation amplifiers, recording system, and ambient electromagnetic signals received by the cables. The signal shown in Figure 11 (a) has been corrupted by power-line interference at 60 Hz and its harmonics and other high frequencies. It can be seen that the proposed algorithm is robust to noise. Moreover, the proposed algorithm is not sensitive to baseline wander and detected the T waves correctly, as shown in Figure 11 (b).

NSR is a normal ECG cycle; it is initiated by the sinoatrial node and consists of a P wave followed, after a brief pause, by a QRS complex and then a T wave [26]. The proposed algorithm correctly detected T waves in three types of normal beats: 1) NSR without U waves (record 100 of the MIT-BIH database), as shown in Figure 11 (c), 2) NSR with U waves (record 103), as shown Figure 11 (d), and 3) NSR with negative polarization (record 108), as shown Figure 11 (e). LBBB results from conduction delays or blocks at any site in the intraventricular conduction system, including the main LBBB and the bundle of His. The result of an LBBB is extensive reorganization of the activation pattern of the left ventricles [26]. The proposed algorithms successfully detected normal and merged P and T waves in two types of LBBBs: 1) LBBB beats with merged P and T waves (record 109), as shown in Figure 11 (f) and 2) LBBB beats with normal T waves (record 111), as shown in Figure 11 (g). However, RBBB is a result of a conduction delay in a portion of the right-sided intra-ventricular conduction system. The delay can occur in the main RBBB itself, in the bundle of His, or in the distal right ventricular conduction system. RBBBs may be caused by a minor trauma, such as right ventricular catheterization [26]. As shown in Figure 11 (h), the proposed algorithms succeeded in detecting the T waves in ECG signals of RBBB (record 118).

PVCs are characterized by the premature occurrence of a QRS complex that is abnormal in shape and that has a longer duration than normal QRS complexes, generally exceeding 120 ms. The T wave is commonly large and opposite in direction to the major deflection of the QRS. The QRS complex is generally not preceded by a P wave, but it can be preceded by a non-conducted sinus P wave occurring

at the expected time [26]. In Figure 11 (i), a special case of PVC is shown, called bigeminy, where the premature ventricular beats occur after every normal beat in an alternating pattern. The proposed algorithm succeeded in detecting the T waves in the normal beats and the T waves in the premature ventricular beats (record 200). PACs are among the most common causes of irregular pulses and can originate from any area in the heart [26]. The impulse is discharged prematurely by an irritable focus in the atria giving rise to a distorted P wave, usually superimposed on the preceding T wave. As shown in Figure 11 (j), the proposed algorithms detected the merged T waves in PACs (record 209).

As illustrated in Figure 11, the proposed method successfully detected T waves in ECG signals with a low SNR, baseline wander, and various arrhythmias. The performance of the T-wave detection algorithms is evaluated using two statistical measures: $SE = TP/(TP + FN)$ and $+P = TP/(TP + FP)$, where TP is the number of true positives (T wave detected as T wave), FN is the number of false negatives (T wave has not been detected), and FP is the number of false positives (non-T wave detected as T wave). The sensitivity SE reports the percentage of true beats that were correctly detected by the algorithm. The positive predictivity +P reports the percentage of beat detections that were true beats.

The abnormal heart rhythms caused a large number of FNs compared to the FPs. Table 1 shows the result of T-wave detection over 48 records of the MIT-BIH database. FNs are mainly caused by noise and PVC, as in record 219, and atrial fibrillation, as in record 202. The algorithm achieved a sensitivity of 99.86% and a positive predictivity of 99.65%, which are promising results for handling the non-stationary effects, low SNR, PACs, PVCs, LBBBs, and RBBBs in ECG signals.

Comparison of Performance on the QT Database

As the MIT-BIH is self-annotated, the validation of the detector must be done using a standard annotated database. For this purpose the easily-available QT database [27] is used. This database was annotated by two cardiologists and includes different morphologies such as ST change, supraventricular arrhythmia, normal sinus rhythm, sudden death, and long term. The annotation file of the QT database includes the T peak, onset, and offset. In this work, the T peaks of the whole QT database are used for validation.

The detection performance on the QT database obtained by the proposed T-waves detector record by record performance is shown in Table 2. The overall comparison of our results with the existing T-wave detection algorithms on the QT database is demonstrated in Table 3. It summarizes the performances in terms of number of beats, methodology, SE, and +P. Martínez *et al.* [28] and Laguna *et al.* [29]

scored slightly higher overall performances (average of SE and +P) than the proposed algorithm. This is because they used only 3,542 heart beats from the QT database, and therefore, their algorithms are not superior in terms of performance. It is clear that the proposed algorithm succeeds in handling long ECG recordings with high performance over 111,201 heart beats compared to the well-known publications for T-wave detection. Moreover, the proposed T-wave detector has not been re-tuned over any databases, thus the results are promising, and the algorithm can detect T peaks over different databases, sampling frequencies, types of arrhythmias, and noise.

Limitations of Study and Future Work

It is important to note that the MIT-BIH database is annotated by one annotator as the results are likely influenced by this. Thus, a second annotation is required; however, annotating P and T waves is a difficult task due to inter-annotator discrepancy, as the two annotators will never agree completely on what and how to annotate the P and T waves in each record. The preliminary results are promising, especially after testing the algorithm on the QT database; however, more testing is necessary to generalize the findings.

One of the next steps regarding the results of this study is to detect arrhythmic ECG beats using the RT or ST interval as a main feature. In addition, the detection of P waves based on the accurate detection of T-wave peaks needs to be examined. Moreover, perhaps, an optimization over the clinical parameters after splitting the databases into a training set and test set may improve the detection rate of the T waves.

Technically, exploring the event-related moving average methodology for detecting events in ECG signals is promising in terms of computational complexity and efficiency. This can be further improved by investigating other bandpass filters with different orders and also by developing fast-moving average techniques for real-time analysis and mobile phone applications.

Conclusions

There is a limitation when evaluating T-wave detection algorithms as finding datasets with annotated T waves is quite difficult. Consequently, comparing the existing algorithms becomes even more difficult.

Therefore, annotation of T waves is discussed and provided. The use of two moving averages is simple and computationally efficient for mobile electronic health tools, such as cell phones and telemedicine technologies. The assessment of the T detector has been reliably done over the existing standard databases (QT and MIT-BIH), which contain different beat types and morphologies found in ECG signals. The developed algorithm was evaluated on all ECG recordings in the MIT-BIH database, 48 self-annotated records containing a total of 109,985 heart beats. It achieved a sensitivity of 95% and a positive predictivity of 98.59% over the MIT-BIH ECG signals, which contain low SNR, baseline wander, paced beats, and various arrhythmias. Interestingly, the proposed algorithm succeeds to score high overall performance (accuracy of 96.7%) over the QT database (111,201 heart beats). Overall, simplicity and efficiency are required in developing T detection algorithms for processing long-term recordings and large databases as well as for expanding our telemedicine capabilities in the near future.

Acknowledgments

Mohamed Elgendi gratefully acknowledges the Australian government and Charles Darwin University whose generous scholarships facilitated this research. He appreciates the support of Prof. Friso De Boer and acknowledges Dr. Gari Clifford for helpful discussions.

References

1. Dilaveris PE, Gialafos EJ, Sideris SK, Theopistou AM, Andrikopoulos GK, et al. (1998) Simple electrocardiographic markers for the prediction of paroxysmal idiopathic atrial fibrillation. *American Heart Journal* 135: 733–738.
2. Goutas A, Ferdi Y, Herbeuval JP, Boudraa M, Boucheham B (2005) Digital fractional order differentiation-based algorithm for P and T-waves detection and delineation. *ITBM-RBM Elsevier* 26.
3. Ren-Guey L, Yih-Chien C, Chun-Chieh H, Chwan-Lu T (2007) A mobile care system with alert mechanism. *IEEE Transactions on Information Technology in Biomedicine* 11: 507–517.

4. Rasid MFA, Woodward B (2005) Bluetooth telemedicine processor for multichannel biomedical signal transmission via mobile cellular networks. *IEEE Transactions on Information Technology in Biomedicine* 9: 35–43.
5. Wen C, Yeh MF, Chang KC, Lee RG (2008) Real-time ECG telemonitoring system design with mobile phone platform. *Measurement* 41: 463–470.
6. Gradl S, Kugler P, Lohmuller C, Eskofier B (2012) Real-time ECG monitoring and arrhythmia detection using Android-based mobile devices. In: *Proc. Ann Int. Conf. IEEE Engineering in Medicine and Biology Society (EMBC)*, 28 Aug–1 Sept, 2012, San Diego, CA, USA, pp. 2452–2455.
7. Scully C, Jinseok L, Meyer J, Gorbach AM, Granquist-Fraser D, et al. (2012) Physiological parameter monitoring from optical recordings with a mobile phone. *IEEE Transactions on Biomedical Engineering* 59: 303–306.
8. Elgendi M, Eskofier B, Dokos S, Abbott D (2014) Revisiting QRS detection methodologies for portable, wearable, battery-operated, and wireless ECG systems. *PLoS ONE* 9: e84018.
9. Oresko J (2010) Portable heart attack warning system by monitoring the ST segment via smartphone electrocardiogram processing. Ph.D. thesis, University of Pittsburgh.
10. Moody GB, Mark RG (2001) The impact of the MIT-BIH arrhythmia database. *IEEE Engineering in Medicine and Biology Magazine* 20: 45–50.
11. Goldberger AL, Amaral LAN, Glass L, Hausdorff JM, Ivanov PC, et al. (2000) PhysioBank, PhysioToolkit, and PhysioNet: Components of a new research resource for complex physiologic signals. *Circulation* 101: e215–e220.
12. Willems JL, Arnaud P, Bommel JHV, Bourdillon PJ, Degani R, et al. (1987) A reference data base for multilead electrocardiographic computer measurement programs. *Journal of the American College of Cardiology* 10: 1313–1321.
13. Elgendi M (2013) Fast QRS detection with an optimized knowledge-based method: Evaluation on 11 standard ECG databases. *PLoS ONE* 8: e73557.

14. Elgendi M, Jonkman M, De Boer F (2010) Frequency bands effects on QRS detection. In: the 3rd International Conference on Bio-inspired Systems and Signal Processing (BIOSIGNALS2010), January 20–23, 2010, Valencia, Spain, pp. 428–431.
15. Elgendi M, Norton I, Brearley M, Abbott D, Schuurmans D (2013) Systolic peak detection in acceleration photoplethysmograms measured from emergency responders in tropical conditions. PLoS ONE 8: e76585.
16. Elgendi M, Jonkman M, De Boer F (2010) Heart rate variability measurement using the second derivative photoplethysmogram. In: the 3rd International Conference on Bio-inspired Systems and Signal Processing (BIOSIGNALS2010), January 20–23, 2010, Valencia, Spain, pp. 82–87.
17. Elgendi M (2013). Detection of *a* and *b* waves in acceleration photoplethysmogram, <http://vixra.org/abs/1301.0053>.
18. Elgendi M, Jonkman M, De Boer F (2011) Heart rate variability and acceleration plethysmogram measured at rest. In: Fred A, Filipe J, Gamboa H, editors, Biomedical Engineering Systems and Technologies, Springer, Communications in Computer and Information Science. pp. 266–277.
19. Elgendi M, Jonkman M, De Boer F (2009) Measurement of *a-a* intervals at rest in the second derivative plethysmogram. In: the IEEE Conference in Bioelectronics and Bioinformatics, Dec 9–11, 2009, RMIT, Melbourne, Australia, pp. 75–79.
20. Sahambi JS, Tandon SN, Bhatt RKP (1997) Using wavelet transforms for ecg characterization. an on-line digital signal processing system. IEEE Engineering in Medicine and Biology Magazine 16: 77–83.
21. Roskamm H, Csapo G (1982) Disorders of cardiac function. New York: Dekker, 1st edition.
22. Elgendi M, Jonkman M, De Boer F (2009) Recognition of T waves in ECG signals. In: Proc. IEEE 35th Annual Northeast Bioengineering Conference, Boston, MA, USA. pp. 1–2.
23. Trahanias P (1993) An approach to QRS complex detection using mathematical morphology. IEEE Transactions on Biomedical Engineering 40: 201–205.

24. Laguna P, Thakor N, Caminal P, Jan R, Yoon HR, et al. (1990) New algorithm for qt interval analysis in 24-hour holter ecg: performance and applications. *Medical and Biological Engineering and Computing* 28: 67–73.
25. Schimpf R, Wolpert C, Bianchi F, Giustetto C, Gaita F, et al. (2003) Congenital short qt syndrome and implantable cardioverter defibrillator treatment: inherent risk for inappropriate shock delivery. *Journal of Cardiovascular Electrophysiology* 14: 1273–1277.
26. Braunwald E, Zipes D, Libby P, Bonow R (2004) *Braunwald’s Heart Disease: A Textbook of Cardiovascular Medicine*. Philadelphia: Saunders, 7th edition.
27. Laguna P, Mark RG, Goldberg A, Moody GB (1997) A database for evaluation of algorithms for measurement of QT and other waveform intervals in the ECG. In: *Proc. IEEE Computers in Cardiology*, Sept 7–10, 1997, Lund, Sweden, pp. 673–676.
28. Martínez JP, Almeida R, Olmos S, Rocha AP, Laguna P (2004) A wavelet-based ECG delineator: evaluation on standard databases. *IEEE Transactions on Biomedical Engineering* 51: 570–581.
29. Laguna P, Jané R, Caminal P (1994) Automatic detection of wave boundaries in multilead ECG signals: validation with the CSE database. *Computers and Biomedical Research* 27: 45–60.
30. Vila J, Gang Y, Presedo J, Fernandez-Delgado M, Barro S, et al. (2000) A new approach for TU complex characterization. *IEEE Transactions on Biomedical Engineering* 47: 764–772.

Tables

Table 1. T-wave peak detection performance over the annotated MIT-BIH arrhythmia database [10, 11]. To evaluate the performance of the T-wave detection algorithm, two statistical measures are used: $SE = TP/(TP + FN)$ and $+P = TP/(TP + FP)$, where TP is the number of true positives (T wave detected as T wave), FN is the number of false negatives (T wave has not been detected), and FP is the number of false positives (non-T wave detected as T wave).

Record	No of beats	TP	FP	FN	SE (%)	+P (%)
100	2274	2272	0	0	100.00	100.00
101	1866	1863	1	4	99.79	99.95
102	2187	2185	0	0	100.00	100.00
103	2084	2082	0	4	99.81	100.00
104	2229	2227	0	1	99.96	100.00
105	2602	2586	0	2	99.92	100.00
106	2026	2024	0	56	97.23	100.00
107	2136	2134	0	3	99.86	100.00
108	1763	1757	0	13	99.26	100.00
109	2533	2530	0	0	100.00	100.00
111	2123	2121	0	16	99.25	100.00
112	2539	2537	0	0	100.00	100.00
113	1794	1792	0	0	100.00	100.00
114	1890	1885	0	69	96.34	100.00
115	1953	1951	0	19	99.03	100.00
116	2395	2392	0	2	99.92	100.00
117	1535	1533	0	0	100.00	100.00
118	2278	2276	0	4	99.82	100.00
119	1988	1986	0	4	99.80	100.00
121	1863	1860	0	46	97.53	100.00
122	2476	2474	0	0	100.00	100.00
123	1519	1517	0	0	100.00	100.00
124	1619	1617	0	7	99.57	100.00
200	2601	2599	0	9	99.65	100.00
201	1949	1947	0	57	97.07	100.00
202	2138	2134	0	113	94.70	100.00
203	2988	2965	0	1	99.97	100.00
205	2656	2556	0	0	100.00	100.00
207	2324	2139	0	9	99.58	100.00
208	2953	2949	0	0	100.00	100.00
209	3006	3003	0	5	99.83	100.00
210	2652	2637	0	0	100.00	100.00
212	2748	2746	0	0	100.00	100.00
213	3250	3247	0	0	100.00	100.00
214	2262	2184	0	0	100.00	100.00
215	3362	3354	0	0	100.00	100.00
217	2208	2205	0	3	99.86	100.00
219	2154	2152	0	144	93.31	100.00
220	2048	2046	0	2	99.90	100.00
221	2427	2424	0	0	100.00	100.00
222	2485	2472	0	33	98.67	100.00
223	2604	2601	0	1	99.96	100.00
228	2060	2056	0	52	97.47	100.00
230	2256	2254	0	39	98.27	100.00
231	1571	1569	0	0	100.00	100.00
232	1783	1781	0	1	99.94	100.00
233	3077	2914	0	1	99.97	100.00
234	2751	2749	0	0	100.00	100.00
	109985	109284	1	720	99.28	100.00

Table 2. T-wave peak detection performance over the annotated QT database [27]. To evaluate the performance of the T-wave detection algorithm, two statistical measures are used: $SE = TP/(TP + FN)$ and $+P = TP/(TP + FP)$, where TP is the number of true positives (T wave detected as T wave), FN is the number of false negatives (T wave has not been detected), and FP is the number of false positives (non-T wave detected as T wave).

Record	No of beats	TP	FP	FN	SE (%)	+P (%)
sel100	1134	1132	0	1	99.91	100.00
sel102	1088	1086	0	2	99.82	100.00
sel103	1048	1046	4	5	99.52	99.62
sel104	1109	1107	9	10	99.10	99.19
sel114	867	864	1	7	99.19	99.88
sel116	1186	1184	0	25	97.89	100.00
sel117	766	764	0	1	99.87	100.00
sel123	756	754	0	0	100.00	100.00
sel213	1641	1639	1	2	99.88	99.94
sel221	1247	1244	0	116	90.68	100.00
sel223	1309	1307	0	6	99.54	100.00
sel230	1077	1075	115	200	81.41	88.40
sel231	732	730	0	1	99.86	100.00
sel232	866	864	18	19	97.80	97.92
sel233	1532	1265	13	112	91.79	98.97
sel301	1352	1348	0	0	100.00	100.00
sel302	1501	1498	1	2	99.87	99.93
sel306	1040	1038	0	30	97.11	100.00
sel307	853	851	0	1	99.88	100.00
sel308	1294	1292	19	21	98.38	98.53
sel310	2012	2008	0	3	99.85	100.00
sel803	1026	1024	0	84	91.80	100.00
sel808	903	901	24	29	96.78	97.32
sel811	704	702	0	1	99.86	100.00
sel820	1159	1157	1	3	99.74	99.91
sel821	1557	1555	2	3	99.81	99.87
sel840	1180	1178	1	2	99.83	99.92
sel847	803	799	0	3	99.62	100.00
sel853	1113	1110	6	8	99.28	99.46
sel871	917	915	2	3	99.67	99.78
sel872	990	988	0	2	99.80	100.00
sel873	859	857	0	1	99.88	100.00
sel883	892	890	30	36	95.96	96.61
sel891	1267	1265	0	1	99.92	100.00
sel16265	1031	1029	10	11	98.93	99.03
sel16272	851	849	0	1	99.88	100.00
sel16273	1112	1110	4	5	99.55	99.64
sel16420	1063	1061	0	1	99.91	100.00
sel16483	1087	1085	1	2	99.82	99.91
sel16539	922	920	0	1	99.89	100.00
sel16773	1008	1006	168	328	67.43	80.17
sel16786	925	923	0	1	99.89	100.00
sel16795	761	759	0	1	99.87	100.00
sel17453	1047	1045	0	1	99.90	100.00
sel0104	804	802	0	1	99.88	100.00
sel0106	897	894	0	1	99.89	100.00
sel0107	823	810	25	34	95.81	96.88
sel0110	872	870	1	3	99.66	99.88
sel0111	908	906	1	1	99.89	99.89
sel0112	684	682	121	189	72.33	80.33
sel0114	698	696	23	28	95.98	96.68
sel0116	560	557	1	3	99.46	99.82
sel0121	1434	1432	2	2	99.86	99.86
sel0122	1414	1412	0	1	99.93	100.00
sel0124	1121	1119	4	5	99.55	99.64
sel0126	945	943	83	793	16.00	64.53
sel0129	672	670	40	55	91.80	93.90
sel0133	840	838	0	1	99.88	100.00
sel0136	810	808	3	4	99.51	99.63
sel0166	813	811	0	1	99.88	100.00
sel0170	897	895	0	1	99.89	100.00
sel0203	1246	1244	0	4	99.68	100.00
sel0210	1063	1061	0	1	99.91	100.00
sel0211	1575	1573	0	1	99.94	100.00
sel0303	1045	1043	1	2	99.81	99.90
sel0405	1216	1214	0	57	95.30	100.00
sel0406	959	957	0	1	99.90	100.00
sel0409	1737	1735	0	1	99.94	100.00
sel0411	1202	1200	0	2	99.83	100.00
sel0509	1028	1026	0	39	96.20	100.00
sel0603	869	867	30	84	90.33	96.32
sel0604	1031	1029	0	2	99.81	100.00
sel0606	1442	1440	0	4	99.72	100.00
sel0607	1184	1182	0	0	100.00	100.00
sel0609	1127	1125	3	4	99.64	99.73
sel0612	751	749	0	1	99.87	100.00
sel0704	1094	1092	0	214	80.40	100.00
sel10	1018	1014	0	3	99.70	100.00
sel11	1087	1084	45	385	64.52	93.96
sel12	1196	1194	0	3	99.75	100.00
sel13	527	525	0	4	99.24	100.00
sel14	897	895	0	0	100.00	100.00
sel15	882	880	0	384	56.36	100.00
sel16	948	946	135	227	76.03	84.21
sel17	682	679	0	511	24.74	100.00
sel18	1563	1561	0	0	100.00	100.00
sel40	1171	1169	0	9	99.23	100.00
sel41	1069	1067	0	24	97.75	100.00
sel42	1366	1363	2	24	98.24	99.85
sel43	1247	1245	0	63	94.94	100.00
sel44	1430	1427	0	46	96.78	100.00
sel45	1337	1335	0	57	95.73	100.00
sel46	971	968	66	96	90.09	92.97
sel47	856	854	0	98	88.52	100.00
sel48	886	884	0	88	90.05	100.00
sel49	1398	1396	0	4	99.71	100.00
sel50	833	831	0	4	99.52	100.00
sel51	661	659	0	32	95.14	100.00
sel51	749	747	0	29	96.12	100.00
sel52	1411	1409	0	1	99.93	100.00
sel17152	1628	1626	0	0	100.00	100.00
sel14046	1260	1258	0	0	100.00	100.00
sel14157	1081	1079	0	9	99.17	100.00
sel14172	663	661	0	73	88.96	100.00
sel15814	1036	1034	0	34	96.71	100.00
111201	110696	1016	4840	95.00	98.59	

Table 3. T-waves detection performance comparison on the QT database [27]. (N/R: not reported).

Publication	Method	# beats	SE (%)	+P (%)
This work	Blocks of Interest	111,201	95.0	98.59
Martínez <i>et al.</i> [28]	Wavelet	3,542	99.77	97.79
Laguna <i>et al.</i> [29]	Low-pass-differentiator	3,542	99.0	97.74
Vila <i>et al.</i> [30]	Modelling	3,542	96.2	N/R

Figures

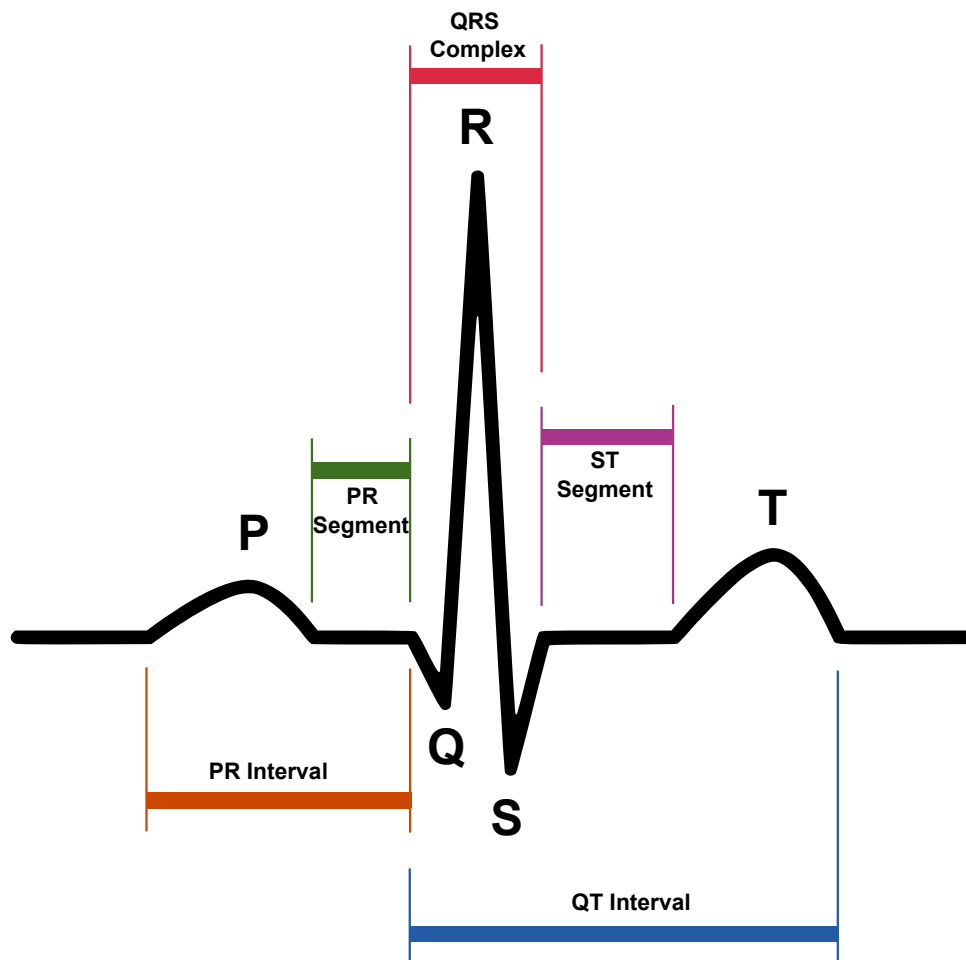


Figure 1. Main Events in ECG signals. A typical ECG trace of the cardiac cycle (one heart beat) consists of a P wave, Q wave, R wave, S wave, and T wave.

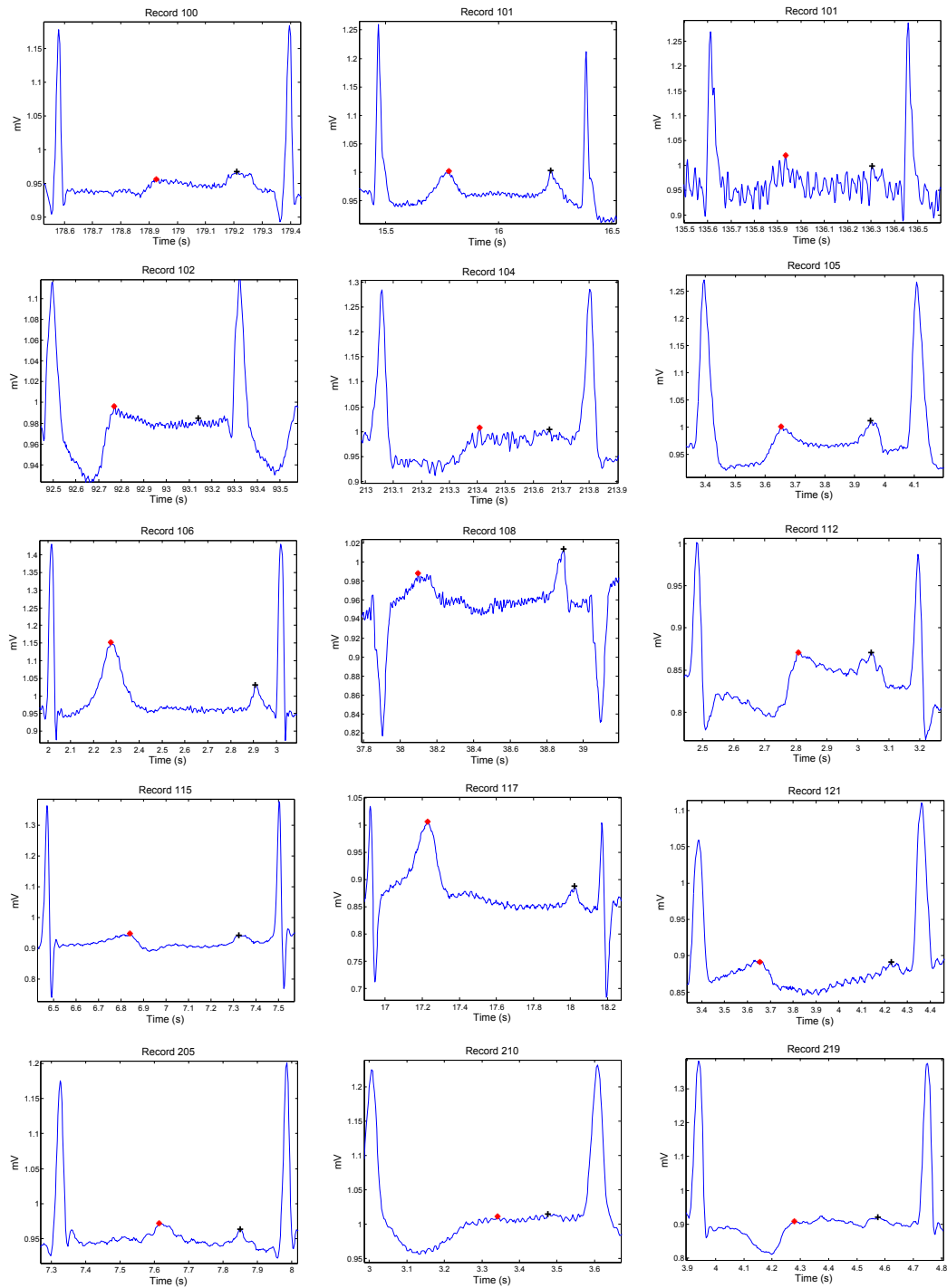


Figure 2. Annotation of P and T waves in normal beats. Here, + represents the P wave and * represents the T wave.

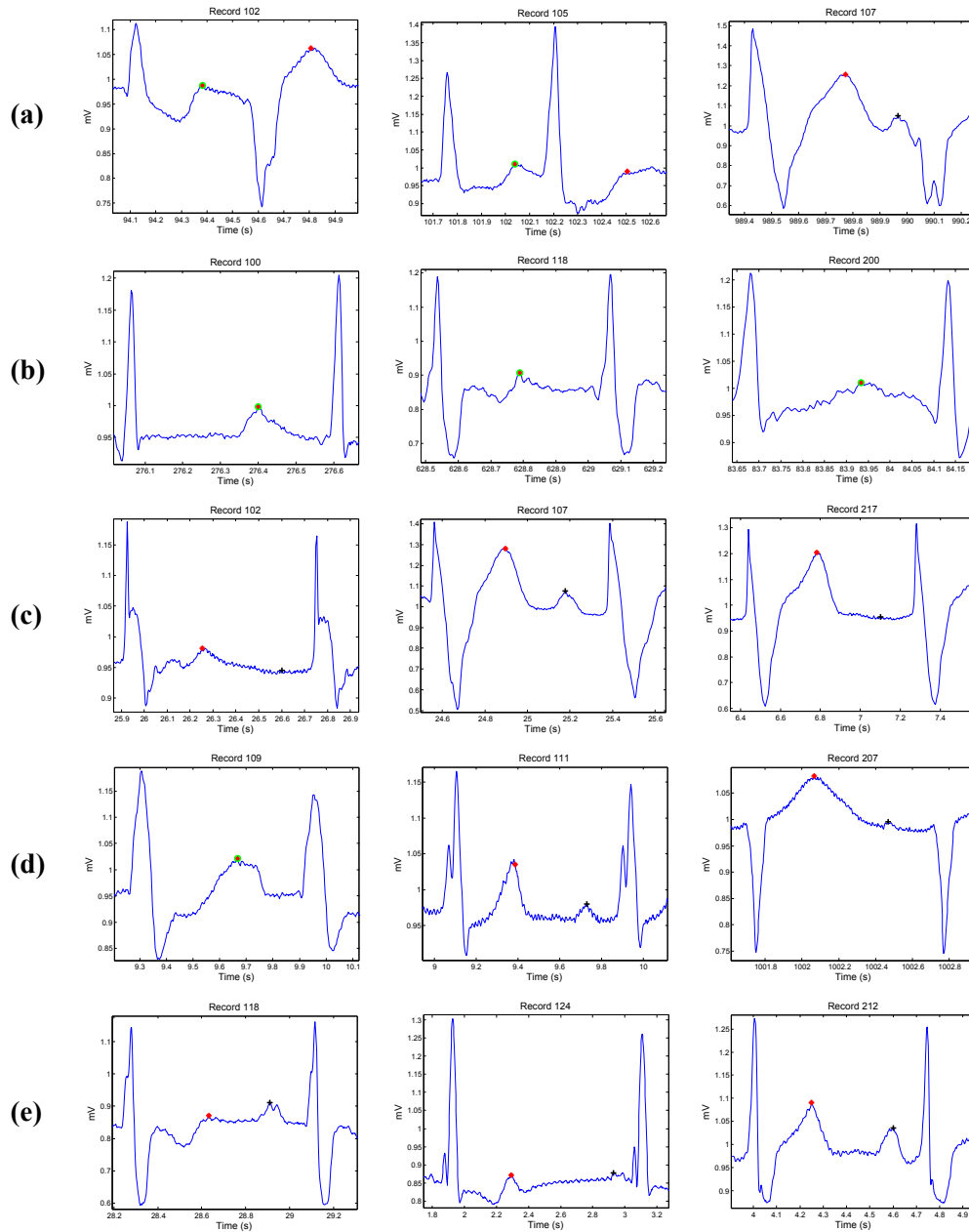


Figure 3. Annotation of Pand T waves in irregular heart beats. Each row contains three different morphologies for a certain type of arrhythmia: (a) premature ventricular beats, (b) premature atrial beats, (c) paced beats, (d) left bundle branch block beats, (e) right bundle branch block beats. Here, + represents the P wave and * represents the T wave, while the green circle with asterisk represents merged P and T waves.

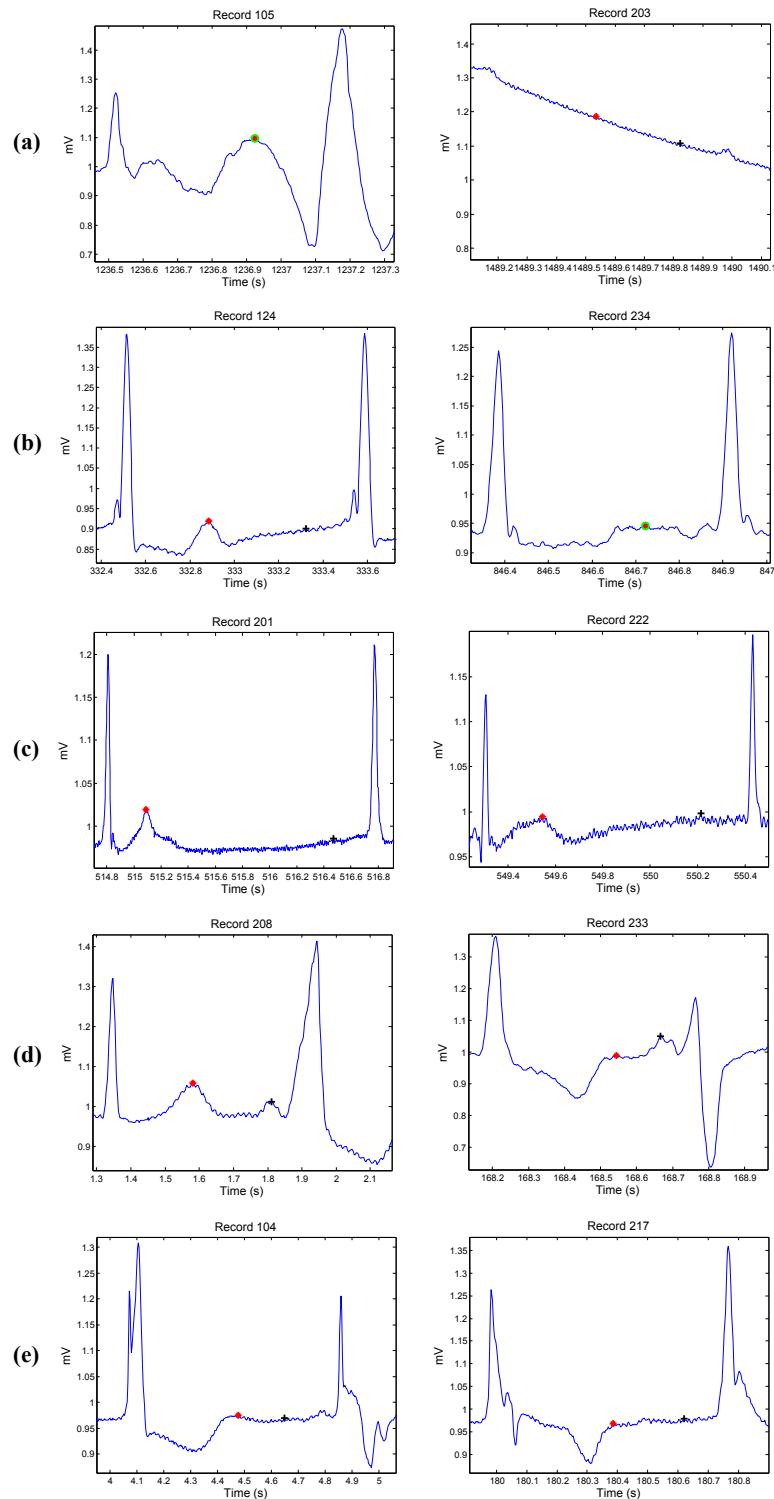


Figure 4. Annotation of P and T waves in unusual beats. Each row contains two different morphologies for a certain type of unusual beats: (a) unclassified beats, (b) nodal premature beat, (c) nodal escape beat, (d) fusion of ventricular and normal beat, (e) fusion of paced and normal beat. Here, + represents the P wave and * represents the T wave, while the green circle with asterisk represents merged P and T waves.

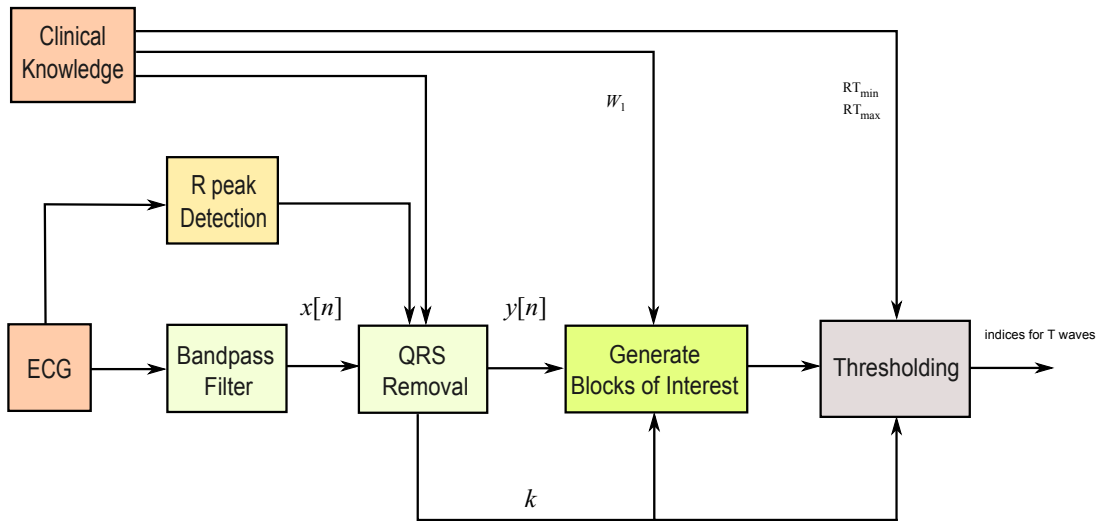


Figure 5. Structure of the T waves detection algorithm. The algorithm consists of four stages: bandpass filter, QRS removal (based on clinical knowledge), feature extraction (generating blocks of interest), and thresholding.

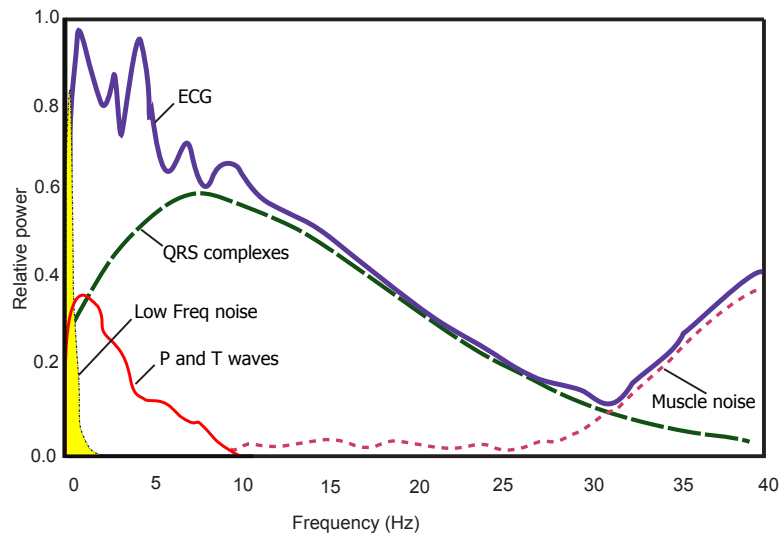


Figure 6. Relative power spectra of noisy ECG signal (100 beats). The optimal frequency band to detect T waves is 0.5–10 Hz.

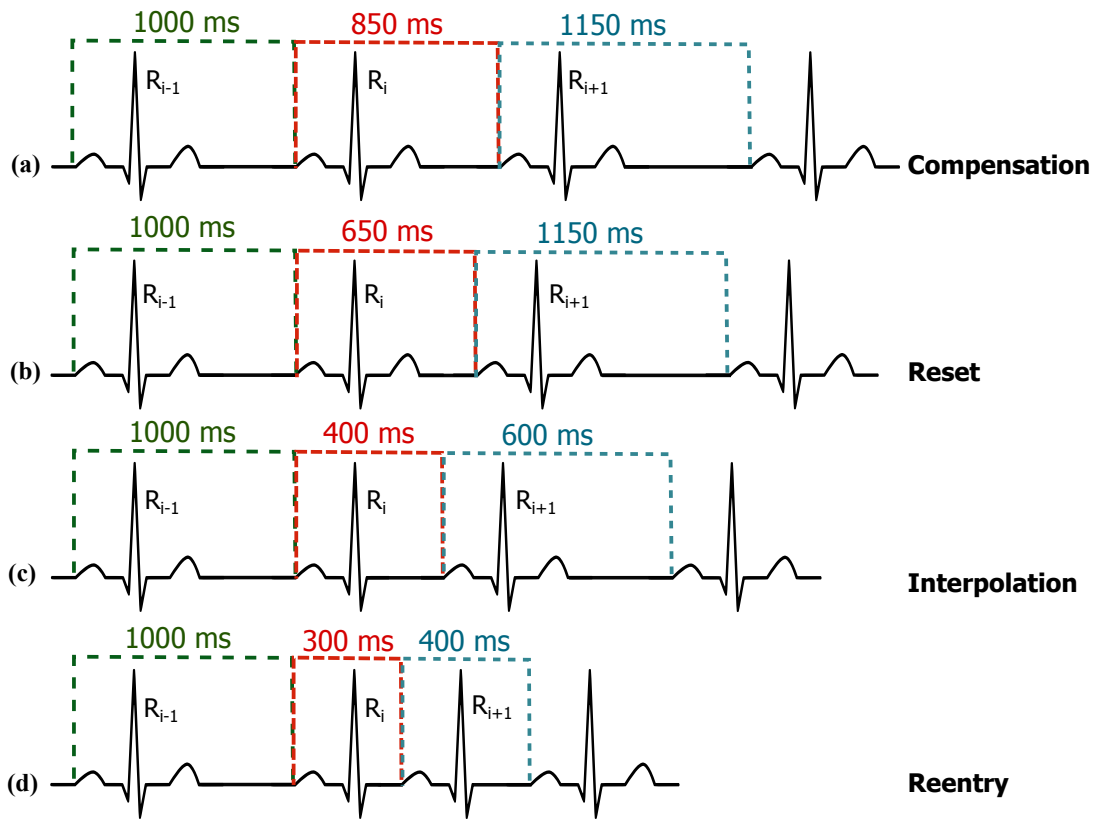


Figure 7. Types of sinus node response to atrial premature depolarization [21].

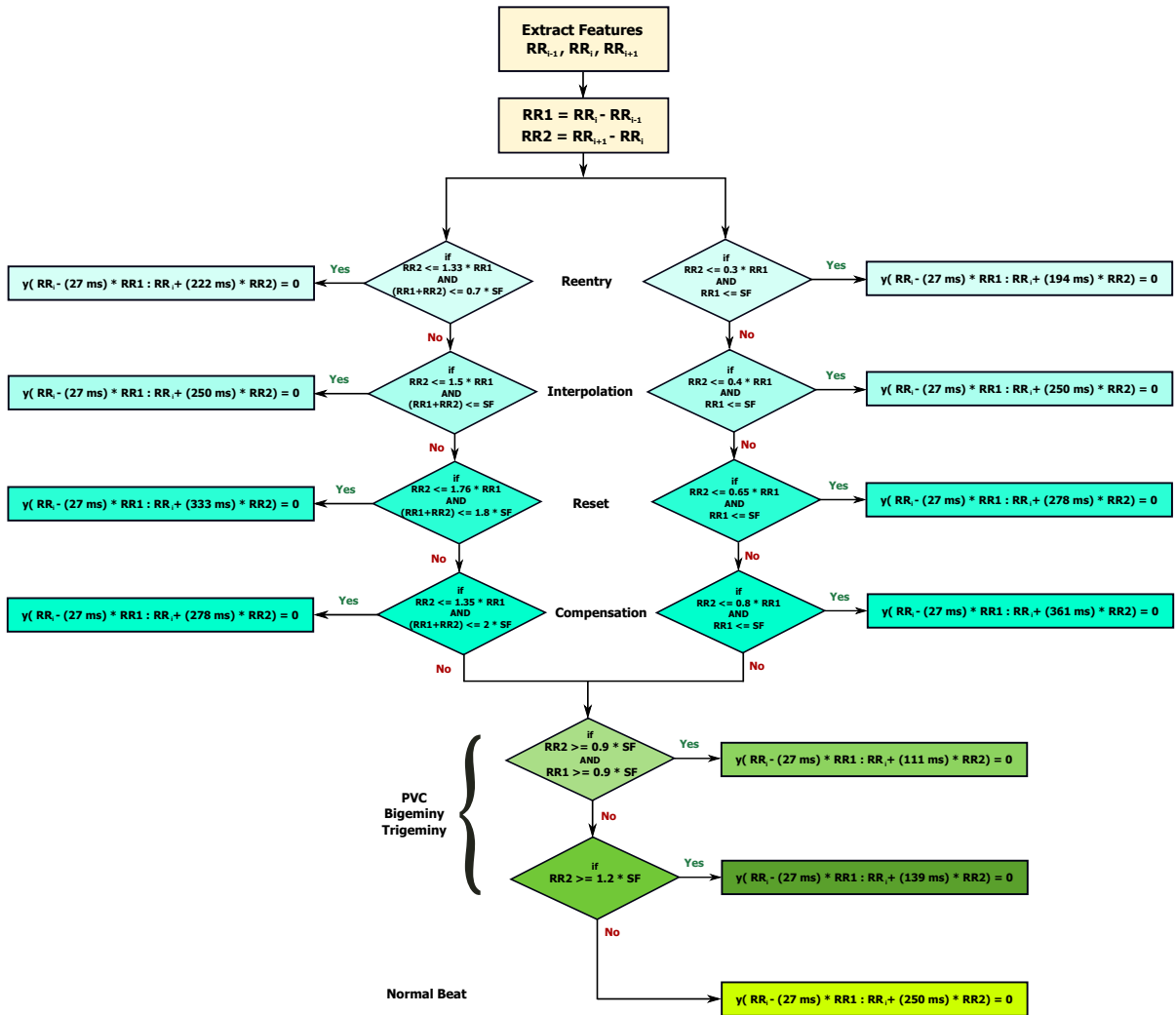


Figure 8. Rule-based knowledge representation of QRS removal based on the clinical knowledge shown in Figure 7.

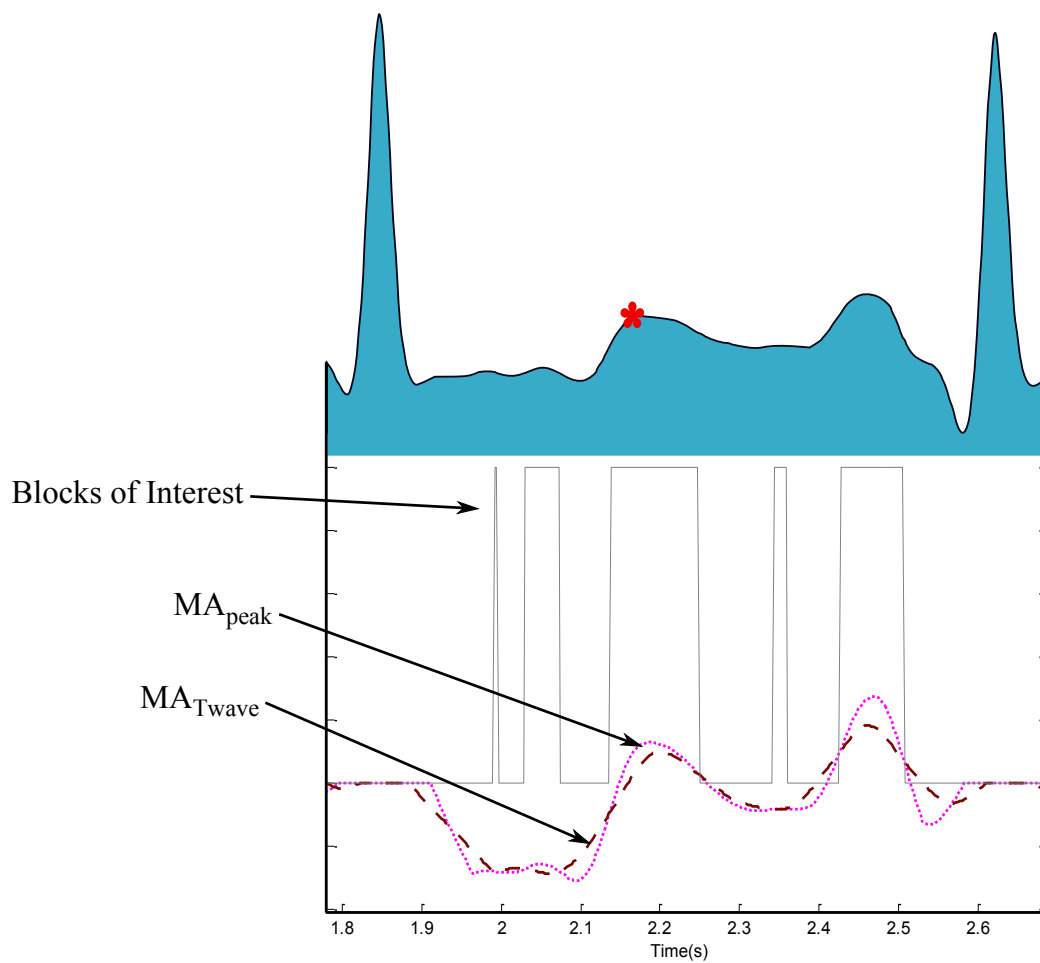


Figure 9. Demonstrating the effectiveness of using two moving averages to detect T waves. The dotted line is the first moving average, while the dashed line is the second moving average.

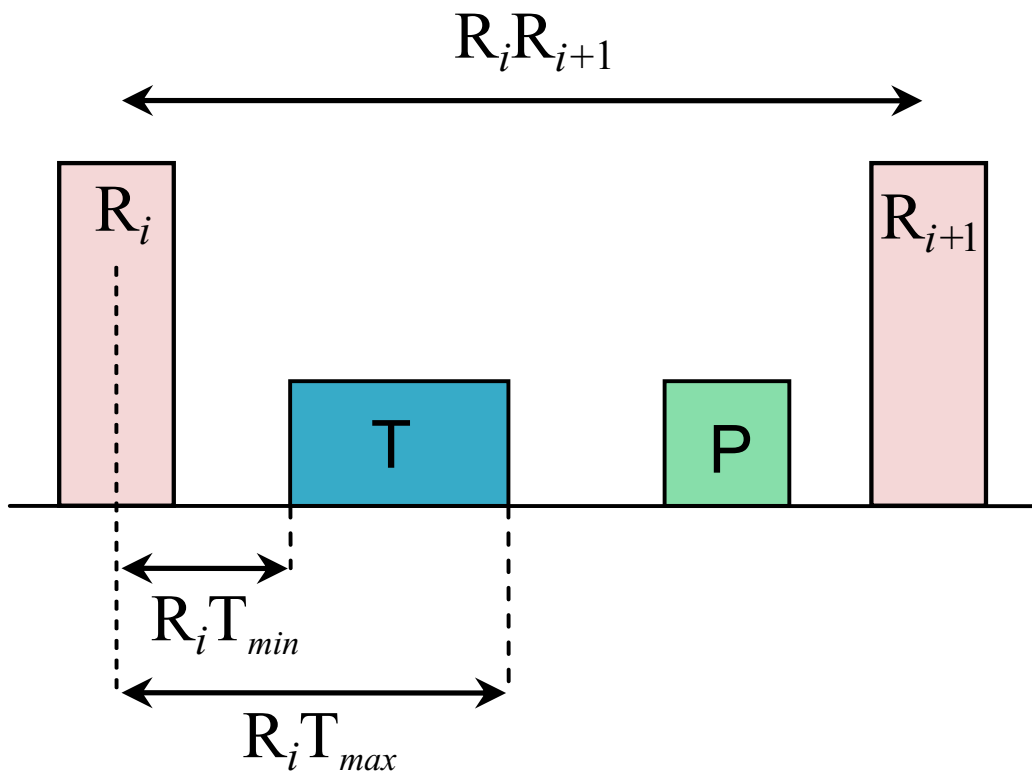


Figure 10. Search regions for T waves in terms of time occurrence with respect to the current R peak (R_i) and the next R peak (R_{i+1}). Where $R_i T_{min}$ represents the minimum interval between the T wave and current R peak and $R_i T_{max}$ represents the maximum interval between the T wave and the current R peak.

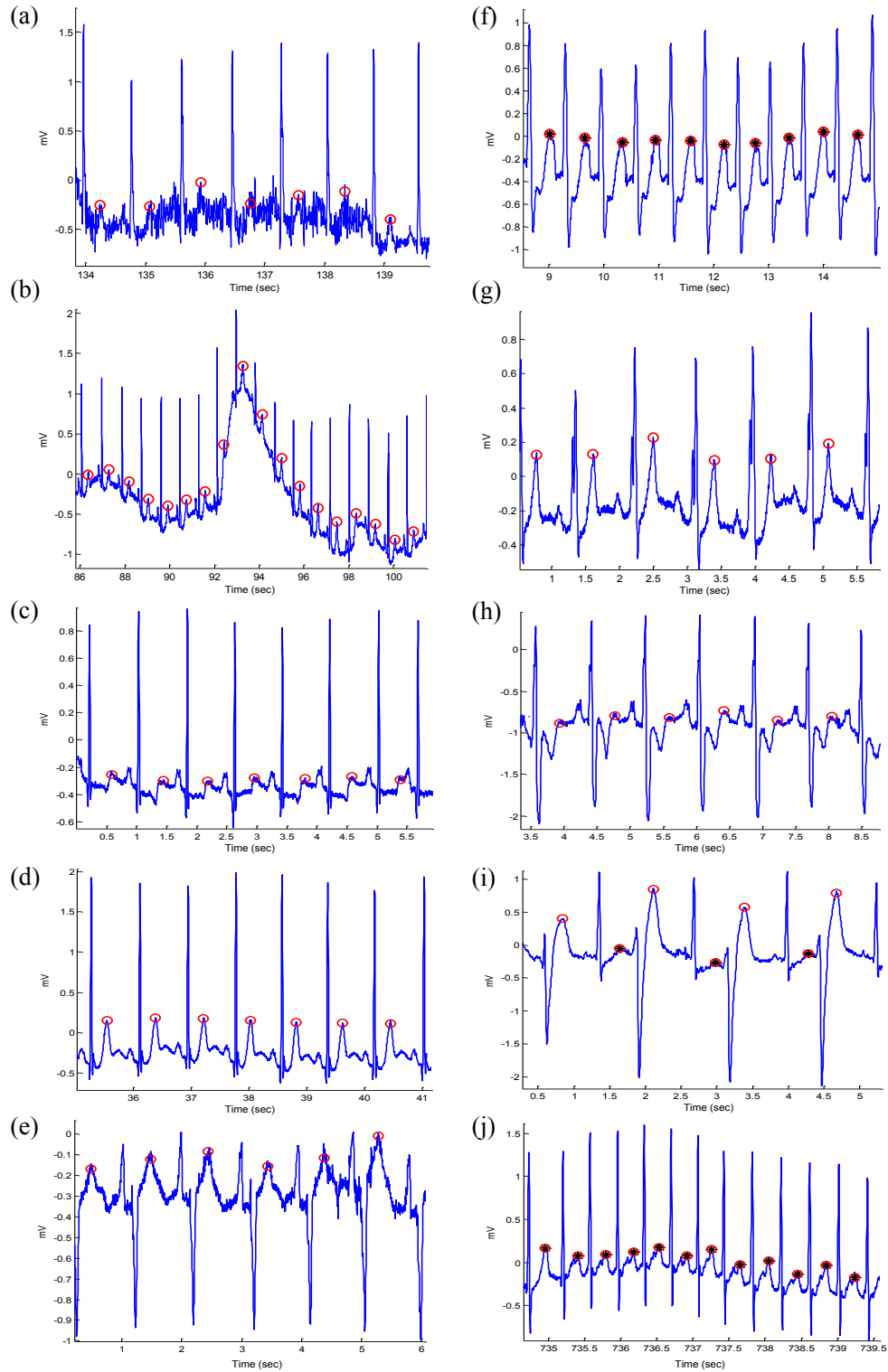


Figure 11. Demonstrating the performance of the proposed T-wave detection algorithm on the MIT-BIH Database. The algorithm succeeds to detect T-wave peaks in ECG signals that contain: (a) high-frequency noise, (b) baseline wander, (c) normal sinus rhythm without U waves, (d) normal sinus rhythm with U waves, (e) normal sinus rhythm with negative polarization, (f) LBBB beats with merged P and T waves, (g) LBBB beats, (h) RBBB beats from record 118, (i) PVC beats from record 200, (j) PAC beats from record 209. Here, the empty red circle represents the detected T wave while the a circle with a black asterisk represents detection of merged P and T waves.